



# AMERICAN METEOROLOGICAL SOCIETY

*Journal of Climate*

## **EARLY ONLINE RELEASE**

This is a preliminary PDF of the author-produced manuscript that has been peer-reviewed and accepted for publication. Since it is being posted so soon after acceptance, it has not yet been copyedited, formatted, or processed by AMS Publications. This preliminary version of the manuscript may be downloaded, distributed, and cited, but please be aware that there will be visual differences and possibly some content differences between this version and the final published version.

The DOI for this manuscript is doi: 10.1175/JCLI-D-16-0198.1

The final published version of this manuscript will replace the preliminary version at the above DOI once it is available.

If you would like to cite this EOR in a separate work, please use the following full citation:

Seviour, W., A. Gnanadesikan, and D. Waugh, 2016: The Transient Response of the Southern Ocean to Stratospheric Ozone Depletion. *J. Climate*. doi:10.1175/JCLI-D-16-0198.1, in press.

© 2016 American Meteorological Society



# **The Transient Response of the Southern Ocean to Stratospheric Ozone**

## **Depletion**

William J. M. Seviour\*, Anand Gnanadesikan, Darryn W. Waugh

*Department of Earth and Planetary Sciences, Johns Hopkins University, Baltimore, Maryland.*

\* *Corresponding author address:* William Seviour, Department of Earth and Planetary Sciences,

Johns Hopkins University, 3400 N. Charles St., Baltimore, MD, 21218.

E-mail: wseviou1@jhu.edu

## ABSTRACT

8    Recent studies have suggested that the response of the Southern Ocean to  
9    stratospheric ozone depletion is nonmonotonic in time; consisting of an initial  
10   cooling followed by a long-term warming. This result may be significant for  
11   the attribution of observed Southern Ocean temperature and sea ice trends,  
12   but the time scale and magnitude of the response is poorly constrained, with a  
13   wide spread among climate models. Furthermore, a long-lived initial cooling  
14   period has only been observed in a model with idealized geometry and lacking  
15   an explicit representation of ozone. Here we calculate the transient response  
16   of the Southern Ocean to a step-change in ozone in a comprehensive coupled  
17   climate model, GFDL ESM2Mc. The Southern Ocean responds to ozone  
18   depletion with an initial cooling, lasting 25 years, followed by a warming. We  
19   extend previous studies to investigate the dependence of the response on the  
20   ozone forcing as well as the regional pattern of this response. The response  
21   of the Southern Ocean relative to natural variability is shown to be largely  
22   independent of the initial state. However, the magnitude of this response is  
23   much less than that of natural variability found in the model, which limits its  
24   influence and detectability.

## 25 **1. Introduction**

26 In recent decades significant trends in the summertime atmospheric circulation over the South-  
27 ern Ocean (SO) have been observed. The extratropical jet has shifted poleward and intensified  
28 (Thompson et al. 2011; Swart and Fyfe 2012; Hande et al. 2012), consistent with a more positive  
29 Southern Annular Mode (SAM). These trends are outside the range of natural variability found  
30 in coupled climate models (Thomas et al. 2015), and have been largely attributed to the impact  
31 of stratospheric ozone depletion (Polvani et al. 2011; Gerber and Son 2014). At the same time,  
32 an increase in Southern Hemisphere sea ice cover has been observed (Comiso and Nishio 2008;  
33 Parkinson and Cavalieri 2012), most prominent in the fall, and in contrast to the large decrease  
34 seen in the Arctic.

35 Several studies have investigated a possible link between these atmospheric and ocean–sea ice  
36 trends. The sea surface temperature (SST) pattern associated with interannual variability in the  
37 SAM is a dipole in the meridional direction, a feature driven largely by horizontal Ekman trans-  
38 port (as well as vertical Ekman pumping in summer (Purich et al. 2016)), and is consistent across  
39 observations and climate models (Watterson 2000; Hall and Visbeck 2002; Sen Gupta and England  
40 2006; Ciasto and Thompson 2008). For the positive phase of the SAM, this pattern gives a warm-  
41 ing in SST at about 40°S and cooling south of about 50°S, leading to an overall increase in SO sea  
42 ice cover (Lefebvre et al. 2004; Lefebvre and Goosse 2008; Purich et al. 2016). Following these  
43 results, Goosse et al. (2009) argued that the ozone-driven trend toward a more positive SAM is the  
44 main driver of the observed SO sea ice expansion. However, this contradicts the results of many  
45 coupled climate model studies which have found a warming of the SO and a reduction in sea ice  
46 extent associated with stratospheric ozone depletion (Sigmond and Fyfe 2010; Bitz and Polvani  
47 2012; Smith et al. 2012; Sigmond and Fyfe 2014; Previdi et al. 2014; Solomon et al. 2015a).

48 Ferreira et al. (2015) (hereafter F15) attempted to reconcile these opposing views by proposing  
49 that the response of the SO to stratospheric ozone depletion has two time scales; a fast and slow  
50 response. They found the fast response to be similar to the interannual SAM-SST correlation,  
51 driven by horizontal Ekman transport, and leading to an increase in sea ice cover. On the other  
52 hand, the slow response was shown to be driven by upwelling of warm water from below the  
53 mixed layer, leading to a reduction in sea ice cover, and consistent with coupled climate modeling  
54 studies. F15 computed the transient ocean response to a step function in ozone depletion in two  
55 coupled climate models: the MITgcm and CCSM3.5. These two simulations had very different  
56 configurations, with the MITgcm using an idealized geometry (Double-Drake), and without an  
57 explicit representation of ozone, while CCSM3.5 is a more comprehensive coupled model with  
58 explicit ozone, realistic geometry, and more sophisticated radiation and cloud schemes. While  
59 F15 showed both models to give a two time scale response, there were also significant differences  
60 between the simulations. The initial cooling period was about 20 years in the MITgcm, but just 5  
61 years in CCSM3.5. Furthermore, the magnitude of the cooling was around three times greater in  
62 the MITgcm than CCSM3.5.

63 More recently, Kostov et al. (2016) investigated the response of the SO to a step increase in the  
64 SAM by studying lagged correlations in preindustrial control simulations included in the Coupled  
65 Model Intercomparison Project Phase 5 (CMIP5). They found a wide range of responses, with  
66 some models giving a two time scale response, but others with persistent cooling. Among those  
67 models which did show a two time scale response there was a wide range of times at which SST  
68 anomalies cross from negative to positive. Better constraining the time scales and magnitudes of  
69 this response will be crucial in determining how much (if any) of the observed sea ice trends may  
70 be attributed to ozone depletion, as well as how ozone recovery may influence future SO changes.

71 In this study, we calculate the transient response of the Southern Ocean to stratospheric ozone  
72 depletion in the Geophysical Fluid Dynamics Laboratory (GFDL) Earth System Model with Mod-  
73 ular Ocean Model (ESM2Mc) coupled climate model. Specifically, we study the response to  
74 a step-change in stratospheric ozone depletion, a similar approach to F15, described in general  
75 terms by Marshall et al. (2014). An advantage of calculating this response is that linear theory  
76 allows the step-function response to be used to predict the response to an arbitrary time-varying  
77 forcing. This approach also allows the mechanisms driving the response to ozone forcing to be  
78 more clearly isolated than if the forcing itself is time-varying. We find an initial cooling lasting  
79 about 25 years, followed by a warming, and a similar magnitude found by F15 for the MITgcm.  
80 This demonstrates that a long-lived cooling such as found for the MITgcm is possible in a climate  
81 model with realistic geometry and explicitly represented ozone. However, this response is small  
82 relative to the natural variability of the model, and only clearly emerges in an ensemble of simu-  
83 lations. We extend F15 to investigate how the response depends on the prescribed ozone forcing  
84 and the initial conditions. We also investigate the spatial structure of the response, showing that  
85 both the time scales and magnitudes of the response vary over the SO.

## 86 **2. Ozone Response Simulations**

87 The GFDL ESM2Mc model (Gnanadesikan et al. 2015) used here is a coarse-resolution version  
88 of GFDL ESM2M (Galbraith et al. 2011; Dunne et al. 2012). The model consists of a  $3.875^\circ \times 3^\circ$   
89 latitude-longitude atmosphere with 24 vertical levels, coupled to a  $3^\circ \times 1.5^\circ$  ocean model with 28  
90 vertical levels. In the ocean model, advection due to geostrophic eddies is parameterized using  
91 a spatially-varying mixing coefficient,  $A_{GM}$  (Gent and McWilliams 1990), which depends on the  
92 horizontal shear between 100 and 2000 m. A minimum coefficient of  $200 \text{ m}^2 \text{ s}^{-1}$  and a maximum  
93 coefficient of  $1400 \text{ m}^2 \text{ s}^{-1}$  are imposed, and the slope-dependent thickness transport also stops

94 increasing at a value of  $0.01A_{GM}$ , to prevent unrealistically large velocities near mixed layers  
95 where slopes become infinite. A lateral eddy mixing coefficient (Redi 1982),  $A_{Redi}$ , with a global  
96 value of  $800 \text{ m}^2 \text{ s}^{-1}$  is also included. A non-local K-profile parameterization scheme (Large et al.  
97 1994) is used for vertical mixing within the ocean boundary layer, and a vertical diffusivity of  
98  $1 \times 10^{-5} \text{ m}^2 \text{ s}^{-1}$  is specified within the ocean interior. Within the mixed layer the model also uses  
99 the parameterization for mixed layer restratification developed by Fox-Kemper et al. (2008). This  
100 parameterization produces an overturning circulation that increases with the mixed layer depth,  
101 the magnitude of the lateral density gradient within the layer, and the radius of deformation.

102 Initial conditions for our simulations are taken from a 500-year-long preindustrial control sim-  
103 ulation using a global carbon dioxide concentration of 286 ppm and ozone concentrations for  
104 the year 1860 from the Stratosphere-troposphere Processes and their Role in Climate (SPARC)  
105 dataset (Cionni et al. 2011). The zonal mean wind stress in this control simulation has a maximum  
106 of 0.15 Pa at the grid point centered at  $49.5^\circ\text{S}$ . If instead the maximum is computed at each lon-  
107 gitude and averaged across the basin, the average latitude is found at  $50.3^\circ\text{S}$ . The maximum wind  
108 stress is essentially identical to the value found in the Ensemble Coupled Data Assimilation prod-  
109 uct (Zhang et al. 2007) as well as the values reported by Large and Yeager (2009). The Antarctic  
110 Circumpolar Current in the model has a transport of 164 Sv through Drake Passage, which is on  
111 the high end of the range of observational estimates (Meijers et al. 2012). In combination, the wind  
112 stress and transport characteristics of the model make it relatively competitive with the 23 models  
113 studied by Meijers et al. (2012). As noted by Galbraith et al. (2011), the model has a relatively  
114 realistic representation of the Southern Annular Mode. The main biases in the ESM2Mc model, in  
115 common with other members of the GFDL CM2 suite (Dunne et al. 2012), stem from a tendency  
116 towards too little cloudiness during the Antarctic summer. This leads to a warm bias in SST and a  
117 low bias in sea ice; in the control model sea ice essentially vanishes during the Antarctic summer

118 (Pradal and Gnanadesikan 2014). During the winter, however, Antarctic sea ice in our model cov-  
119 ers an area of  $15.7 \times 10^6$  km<sup>2</sup>, closer to observations than many other models in the CMIP5 series  
120 (Turner et al. 2013).

121 From this control simulation further simulations are branched in which we instantaneously im-  
122 pose a change to contemporary ozone concentrations, using a zonal-mean climatology from 1995-  
123 2001. These contemporary concentrations are derived from a specified dynamics version of the  
124 Whole Atmosphere Community Climate Model (WACCM-SD), in which temperatures and winds  
125 are nudged to meteorological assimilation analysis results, but chemistry calculated interactively  
126 (Solomon et al. 2015b). Neely et al. (2014) have proposed that the coarse temporal resolution  
127 (monthly-mean) of prescribed ozone used by many simulations leads to an underestimate of the  
128 magnitude of ozone depletion. In order to test this, we impose daily-mean concentrations in half  
129 of the simulations, and monthly means of these daily values in the other half. The seasonal cycle  
130 of polar cap (70°-90°N) column ozone for these imposed ozone concentrations are shown in Fig-  
131 ure 1. Ozone is reduced relative to preindustrial concentrations throughout the year, but the largest  
132 difference between monthly and daily values is seen to occur in the spring (September-November),  
133 and the minimum around October 1st is less pronounced for the monthly-mean ozone than daily-  
134 mean because of the linear interpolation used. The monthly-mean ozone changes imposed here  
135 are similar to those of the SPARC dataset, although with slightly less depletion during the summer  
136 and spring (Figure 1).

137 The SO in GFDL ESM2Mc displays significant multi-decadal variability, a feature seen in sev-  
138 eral, but not all, coupled climate models (de Lavergne et al. 2014; Martin et al. 2013). Figure  
139 2 shows the time series of SO SST for 200 years of the preindustrial control simulation. Multi-  
140 decadal variability is apparent, with a period of approximately 50 years and this variability is  
141 dominated by the Ross and Weddell seas (Figure 2(b)). Variability in these two regions is corre-

lated, but largest in the Weddell Sea, which shows the most extreme minima and maxima. Further investigation shows this variability to be predominantly caused by large deep convective events in these regions, as was previously reported by (Galbraith et al. 2011) in a similar model. We test the dependence of the SO response to ozone depletion on the initial conditions by initializing half of the ozone response simulations with relatively cold SO SST ('cold start') and half relatively warm ('warm start'), as illustrated in Figure 2(a). These initialization dates are clustered around two warm and cold periods, and spaced 5 years apart within each period. Testing the dependence of this response on initial conditions is particularly important because the ability to reconstruct the response to an arbitrary forcing from the step-function response relies on linear theory. A necessary condition of the response being linear is that it is independent of the initial conditions.

In total, we run 24 ozone response simulations, each 48 years long. These are divided into 12 start dates (6 warm start and 6 cold start), with one daily-mean ozone and one monthly-mean ozone simulation initialized on each date. We begin by discussing the ensemble mean response before describing the effects of the differences in ozone forcing and the initial state.

### 3. Results

#### *a. Ensemble Mean Response*

Ozone depletion is seen to cause a rapid increase in zonal wind stress poleward of the climatological maximum, and a small decrease equatorward of it (Figure 3). This is indicative of a poleward shift and intensification of the extratropical jet, seen in both observations over the past few decades (Thompson and Solomon 2002) and climate model simulations of ozone depletion (Gerber and Son 2014). The ensemble mean maximum zonal wind stress anomaly is about 7 mPa, which is less than the 12 mPa found by F15 for both the MITgcm and CCSM3.5. Although a clear

164 increase in zonal wind stress is seen between  $50^{\circ}$ - $65^{\circ}$ S, there is also a large amount of variability,  
165 even in the ensemble mean (Figure 3(b)). This increase is also not zonally symmetric, with the  
166 largest anomalies in the Indian Ocean sector, and weaker values near Western Antarctica.

167 This atmospheric response to ozone depletion leads to a response in the SO. Figure 4 shows the  
168 ensemble mean response of zonal mean SST following the introduction of ozone depletion. Here  
169 anomalies are calculated as the difference from the climatology of the control simulation. The  
170 initial response (years 0-25) consists of a dipole, with cooling between  $50^{\circ}$ - $70^{\circ}$ S and warming  
171 from  $50^{\circ}$ - $35^{\circ}$ S, a pattern which resembles the SST signature of a positive SAM on interannual  
172 time scales (Watterson 2000). After 25 years the structure of this response changes significantly,  
173 to become a monopole, with warming present throughout the region, though it is particularly  
174 strong near the Antarctic continent ( $70^{\circ}$ S). This response greatly resembles that found by F15 for  
175 the MITgcm (see their Figure 5), which switches from a dipole to monopole pattern after about 20  
176 years.

177 The ocean response is not limited to the surface. Figure 5 shows the ensemble mean evolution  
178 of SO temperature with depth following the introduction of ozone depletion. The initial cooling  
179 is confined near the surface, above the summer mixed-layer, but a warming of the subsurface is  
180 present from the start of the simulation, growing deeper with time. The SST warming at about  
181 25 years occurs when this warm subsurface water is entrained into the mixed layer. The statisti-  
182 cal significance of these temperature changes in the context of natural variability is discussed in  
183 Section 3c.

184 The anomalous wind stress shown in Figure 3 also drives an anomalous ocean circulation. Fig-  
185 ure 6(a) shows the Eulerian meridional overturning circulation response to ozone depletion. This  
186 anomalous circulation consists of two cells which closely match the regions of positive and nega-  
187 tive surface wind stress anomalies, with clockwise circulation from approximately  $65^{\circ}$ - $55^{\circ}$ S and

188 counter-clockwise from 55°-30°S. The Eulerian MOC streamlines are approximately vertical in  
189 the interior (as expected by geostrophy), with return flow in the top and bottom Ekman layers. The  
190 equatorward cell has deeper return flow, permitted by the meridional barriers in this region.

191 It is not the Eulerian, but the residual circulation (sum of Eulerian and eddy-induced parame-  
192 terized circulations), which determines the transport of heat. This residual circulation is shown  
193 alongside the Eulerian circulation in Figure 6(b). The maximum anomaly in the residual circu-  
194 lation at about 57°S is statistically significant from zero ( $p < 0.01$  from a two-tailed  $t$ -test), and  
195 is about 75% of the interannual standard deviation of the control simulation at the same location.  
196 Relative to the Eulerian circulation, the eddy-induced circulation is seen to narrow the region of  
197 anomalous upwelling (indicated by a positive meridional gradient in  $\Psi'_{\text{Res}}$ ) to between approxi-  
198 mately 67°-57°S, as well as significantly strengthening the upwelling in this region. This strength-  
199 ening may be surprising since we would expect to see some compensation between changes in the  
200 Eulerian and eddy overturning circulations (Gent 2016, and references therein). This is because an  
201 increased Eulerian overturning would be expected to tilt isopycnals further, leading to higher shear  
202 and larger Gent-McWilliams overturning. This effect is in fact seen at greater depths in the model.  
203 However, the northward motion of lighter water leads to a reduction of convection and shallower  
204 mixed layer depths. Even though there is a slight increase in the lateral density gradient, the net  
205 result is a decline in the parameterized submesoscale overturning associated with Fox-Kemper  
206 et al. (2008) that acts to reinforce the changes in wind-driven overturning. Note that only the  
207 zonal-mean circulation is analyzed here, and the circulation response may have significant zonal  
208 asymmetries, particularly given the zonally asymmetric nature of the wind stress response (Figure  
209 3(c)).

210 Ocean temperature increases with increasing depth below the mixed layer poleward of about  
211 55°S (Figure 6(a)) because of the presence of seasonal sea ice. The upwelling in this region

212 is therefore expected to result in a warming. Figure 7 shows the temperature response in this  
213 upwelling region, near 62°S and 200 m depth (similar results are found at other locations in the  
214 upwelling region). Indeed, a fairly linear increase in temperature can be seen over the length of the  
215 simulation (this trend is statistically significant from zero  $p < 0.01$ ). The depths with the largest  
216 warming trends, from about 50-100 m (Figure 5) are the same as those with the largest vertical  
217 temperature gradients (Figure 6(a)), while weaker trends are seen at greater depths, where the  
218 temperature gradient is smaller. This explains the appearance of a warming growing deeper with  
219 time, shown in Figure 5. It should be noted, however, that vertical advection is not the sole driver  
220 of this temperature trend, and that vertical mixing (both eddy stirring and diapycnal mixing) also  
221 plays an important role. The magnitude of this mixing is determined by the parameterizations  
222 discussed in Section 2. Can this subsurface temperature trend explain the SST warming after  
223 about 25 years (Figure 2)? The average initial (0-20 years) SST response between 50-70°S is  
224 about  $-0.1$  K. If these subsurface temperatures are efficiently entrained into the mixed layer, we  
225 might expect this initial cooling to be offset when subsurface anomalies reach  $+0.1$  K. This occurs  
226 at about 21 years (Figure 7), so there is relatively good agreement in these time scales.

### 227 *b. Influence of the Temporal Resolution of Ozone Forcing*

228 The maximum annual mean wind stress anomaly increases by approximately 50% on changing  
229 from monthly- to daily-mean ozone (Figure 3(a)). This difference, near the peak anomaly at 56°S,  
230 is statistically significant ( $p < 0.01$ ) according to a two-tailed  $t$ -test. In agreement with Neely  
231 et al. (2014), this indicates that linear interpolation between monthly-mean values, such as was  
232 used for the majority of models which contributed to CMIP5 (Gerber and Son 2014), significantly  
233 underestimates the effects of ozone depletion.

234 The difference between simulations with monthly- and daily-mean ozone is not limited to the  
235 atmosphere. Figure 6(b) shows the Eulerian streamfunction at 200 m for the daily- and monthly-  
236 mean ozone simulations. There is an approximately 50% increase in the anomalous circulation  
237 on changing from monthly- to daily-mean ozone, indicating that the effect of the temporal res-  
238 olution of ozone extends to the ocean interior. However, the difference between the daily- and  
239 monthly-mean ozone simulations is much reduced in the residual-mean circulation, indicating  
240 that parameterized eddies are acting to compensate this difference in the Ekman upwelling. Since  
241 the residual circulation determines the transport of heat, we might therefore expect similar temper-  
242 ature responses for the monthly- and daily-mean ozone simulations. Indeed, there is no significant  
243 difference in their temperature trends, as can be seen in Figure 7.

244 We have seen that the differences in ozone forcing lead to a significantly different atmospheric  
245 response and Eulerian ocean circulation. However, the effect of parameterized eddies is to reduce  
246 these differences, leading to a similar subsurface temperature response. The SST responses in the  
247 daily- and monthly-mean ozone simulations are also similar (Figure 8), and their differences are  
248 dwarfed by those between the warm and cold-start simulations.

### 249 *c. Influence of the Initial State*

250 The mean wind stress anomalies are similar for the cold start and warm start simulations (indeed,  
251 they are not statistically significantly different according to a two-tailed  $t$ -test at any latitude),  
252 indicating that the atmospheric response is largely independent of the initial ocean state (Figure  
253 3(a)). However, Figure 8 demonstrates the importance of the initial state in terms of the SST  
254 response; those simulations initialized with relatively warm SST cool over the first 25 years, while  
255 those initialized with cold SST warm. Moreover, both warm- and cold-start simulations show  
256 reversals of these trends at around 25 years (warm-start) and 35 years (cold-start). It is not clear

257 from this figure which part of this behavior is natural (i.e., unforced), and which, if any, is a  
258 forced response to ozone depletion. In order to determine this we study the difference of the ozone  
259 response simulations from the path of natural variability.

260 This path of natural variability could simply be taken to be that of the control simulation, how-  
261 ever, because of the chaotic nature of SST evolution, the control simulation represents just one  
262 instance of a distribution of possible paths. Using this single control simulation path therefore  
263 introduces a large amount of noise into the results, which rapidly swamps any signal. Instead  
264 we aim to determine the path of natural variability from the autocorrelation function of SST over  
265 the 500-year control simulation. This autocorrelation function multiplied by the initial SST then  
266 gives the *expected* path of natural variability of an ensemble initialized with that value. In order  
267 to test this method we select from the control simulation a set of 21 years with warm and cold  
268 SO SST, each of which must be at least one standard deviation from the mean, and spaced at least  
269 5 years apart, to mirror the initialization of the ozone response simulations. The average of the  
270 SST evolution following these years is shown as the dashed lines in Figure 9. As well as this,  
271 the path determined by autocorrelation is shown, along with a 95% uncertainty range due to the  
272 finite length of the control simulation. The dashed lines almost always lie within the uncertainty  
273 range for the autocorrelation, showing that the autocorrelation accurately captures the unforced  
274 SST evolution.

275 The evolution of SST over the SO, Ross Sea, and Weddell Sea following ozone depletion for the  
276 warm- and cold-start ensembles is shown in Figure 10. Also shown is the path of natural variability  
277 (left) and the difference between this response and natural variability (right). In the majority of  
278 cases natural variability is seen to explain the most of the SST evolution, with the SST response  
279 falling within the uncertainty range of natural variability (shaded regions). A clear exception to

280 this is the Ross Sea, particularly the warm start ensemble, which warms strongly after 15 years, in  
281 contrast to the cooling trend of natural variability.

282 Differences of the forced response from natural variability (Figure 10, right) show similar forced  
283 responses regardless of the initial conditions, although there is a large amount of variability. In  
284 almost all cases there is an initial cooling followed by a warming, with the exception of the cold  
285 start ensemble over the SO, which maintains negative anomalies throughout the length of the  
286 simulation. Interestingly, the cold start ensembles remain colder than the warm start even after  
287 the autocorrelation is removed, indicating a possible asymmetry in the responses (this result also  
288 holds pairwise, not just in the ensemble means, with 80% of all cold and warm start pairs having  
289 colder SO anomalies for the cold start simulation). These differences are, however, mostly small  
290 relative to the size of the responses. Importantly, in order to calculate the response to a time-  
291 varying forcing from the step function response it is a necessary condition that this response be  
292 independent of the initial conditions. The result that warm and cold start simulations give largely  
293 similar results therefore supports the step function response approach (Marshall et al. 2014) for  
294 predicting the response to a more realistic ozone forcing. Furthermore, the similarity of the warm  
295 and cold start ensembles (which are subsamples of the total ensemble) to the ensemble mean,  
296 shows that the ensemble mean results are not highly dependent on the ensemble size.

297 Most of the simulations show a decrease in SST anomalies after about 40 years. This indicates  
298 that the SO may not stabilize at a warmer temperature in our simulations, as found by F15, but  
299 rather continues to vary periodically (this periodicity is also visible in Figures 4 and 5). The forced  
300 response may therefore be thought of as a modulation of natural variability.

301 Figure 10 shows some significant regional differences in the forced response to ozone depletion.  
302 First, although natural variability is larger in the Weddell Sea, the Ross Sea shows a stronger forced  
303 response, particularly in the long-term warming. Second, the time scales of the transient response

304 are regionally dependent; the initial cooling lasts about 15 years in the Ross Sea, and about 30 years  
305 in the Weddell Sea. These regional differences in the SST response are further illustrated in Figure  
306 11, which shows maps of SST anomaly over three 15-year periods following the introduction of  
307 ozone depletion. Note that the anomalies in Figure 11 are relative to the climatology of the pre-  
308 ozone depletion control simulation, rather than the autocorrelation which is too noisy to be used at  
309 each grid point. The Ross Sea is seen to warm in both the warm- and cold-start ensembles, while  
310 the Weddell Sea cools in the warm start ensemble, and warms in the cold start ensemble. The net  
311 result is that the warm-start ensemble results in a dipole of SST after 15 years, while the cold start  
312 shows warming throughout the SO. In the ensemble average, the dominant long-term warming  
313 signal is seen to be in the Ross Sea.

314 Sea ice changes largely follow the SST patterns discussed above (Figure 12). In the ensemble  
315 mean, there is little change in sea ice concentrations over the first 15 years, while differences  
316 between the warm- and cold-start simulations are dominated by the Weddell Sea. The long-term  
317 response gives a reduction in sea ice concentrations in the Ross Sea in all cases, with opposite  
318 responses of the Weddell Sea for warm- and cold-start simulations and little overall change in the  
319 ensemble mean.

320 Changes in winter and summer sea ice area are shown in Figure 13. In the ensemble mean, the  
321 area does not change much in either case for the first 20-25 years, but then falls to a minimum at  
322 about 30 years, before increasing again. The peak fractional change in sea ice area is about 10%  
323 in winter and 20% during the summer, the larger fractional summer change coming at the time of  
324 the largest ozone-induced atmospheric anomalies (Thompson et al. 2011). These changes in sea  
325 ice extent are largely consistent with SO SST (Figure 10), although there is not an initial increase  
326 in sea ice, as might be expected from the initial cooling of SST. This may be because the largest  
327 initial SST cooling in the ensemble mean is quite far equatorward in the Ross Sea sector (Figure

328 11, top-left), away from the sea ice edge, and so has little effect on sea ice in this region (Figure  
329 12, top-left). In fact, the the model has a bias towards too little winter sea ice in the Ross Sea  
330 sector compared with observed values, so this SST cooling would likely have a larger effect on  
331 sea ice under a more realistic climatology. An initial increase in winter sea-ice extent might also  
332 be prevented due to a cancellation between the effects of horizontal Ekman transport (driving a  
333 cooling) and vertical Ekman pumping (driving a warming) during this season (Purich et al. 2016),  
334 in turn resulting from seasonal changes in temperature stratification. The recovery of sea ice after  
335 30 years again demonstrates that the SO continues to vary periodically, rather than stabilizing at a  
336 new mean value.

#### 337 **4. Conclusions**

338 In this study we have investigated the transient response of the SO to a step change in strato-  
339 spheric ozone depletion, using a comprehensive coupled climate model, GFDL ESM2Mc. The  
340 main conclusions are as follows:

- 341 1. Ozone depletion causes a poleward shift of the extratropical jet, leading to enhanced zonal  
342 wind stress over much of the SO. Consistent with Neely et al. (2014), we find an approxi-  
343 mately 50% increase in the maximum annual-mean wind stress anomaly on changing from  
344 monthly-mean to daily ozone. This indicates that linear interpolation between monthly mean  
345 values, which fails to capture the sharp ozone minimum near October 1st (Figure 1), leads to a  
346 significant underestimate of the effects of ozone depletion. The effect of the temporal resolu-  
347 tion of prescribed ozone is not limited to the atmosphere; the stronger wind stress anomalies  
348 using daily ozone drive a stronger Eulerian MOC relative to monthly-mean ozone. However,  
349 when considering the residual circulation, which includes the effect of parameterized eddies,  
350 this difference is much reduced. Since the residual circulation determines the advection of

351 heat, there is little difference in ocean temperature between monthly-mean and daily ozone  
352 simulations.

353 2. Following the introduction of ozone depletion, the SO SST cools and then warms after about  
354 25 years, similar to the result found by F15 for the MITgcm. However, in contrast to the  
355 idealized geometry set-up used by F15, we are able to determine the regional responses to  
356 ozone depletion. The longest-lived initial cooling is found in the Weddell Sea, while the  
357 largest warming is in Ross Sea. Observed SO trends over the last 30 years have been highly  
358 regionally dependent (Parkinson and Cavalieri 2012), and this further highlights the need to  
359 study regional responses.

360 3. GFDL ESM2Mc displays significant quasi-periodic natural variability, driven by SO deep  
361 convective events, which is necessary to remove in order to determine the forced response.  
362 After removing this natural variability the response is seen to be largely independent of the  
363 initial conditions (Figure 10). This result is important because in order to construct the re-  
364 sponse to an arbitrary forcing from the step response, it is necessary that this response be  
365 independent of the initial conditions (Marshall et al. 2014).

366 We have shown that wind-driven changes to the ocean residual circulation, as proposed by F15,  
367 play a significant role in driving the SO temperature response to ozone depletion. However, two  
368 further mechanisms are also important. First, changes in vertical stratification, and so convection,  
369 may be driven by both the northward Ekman transport of fresher water, as well as changes in  
370 precipitation arising from a shift in the storm tracks. Second, changes in cloud cover over the SO,  
371 again arising from a shift of the storm tracks, can significantly affect surface radiative heat fluxes  
372 (Grise et al. 2013; Solomon et al. 2015a). A detailed analysis of the relative contributions of these  
373 mechanisms will be carried out in future work.

374 F15 suggested that ozone depletion could have contributed to the observed expansion of sea  
375 ice cover around Antarctica in the last three decades (Parkinson and Cavalieri 2012). Indeed,  
376 given the initial 25-year cooling seen in this study, similar to that found by F15, our results might  
377 appear to support their conclusions (although we do not find an initial increase in sea ice extent).  
378 However, it should be noted that the magnitude of the forced SO SST response found here is small  
379 compared to natural variability. The initial annual-mean SO cooling found here is about 0.1 K,  
380 but the interannual standard deviation of SO SST in GFDL ESM2Mc is 0.4 K. Hence, it would  
381 take approximately 20 years to detect this forced signal (at the 95% confidence level, using a two-  
382 tailed  $t$ -test), which is not much less than the duration of the signal itself. This calculation only  
383 includes interannual variability, and multi-decadal variability would likely make detection more  
384 difficult. Moreover, the time required to detect the response to a realistic ozone forcing, rather than  
385 a step-function change would be longer still. The interannual standard deviation of SO SST in the  
386 MITgcm simulation analyzed by F15 is similar to that of GFDL ESM2Mc (David Ferreira, pers.  
387 comm.), though it is less periodic. The magnitude of the forced response is also similar, hence we  
388 might expect a similar time scale to detect a signal in the MITgcm.

389 These results highlight the crucial role of SO natural variability in determining the detectabil-  
390 ity of ozone depletion-driven changes. Some recent studies have found parameterized mixing to  
391 significantly affect model SO variability (Heuzé et al. 2015; Kjellsson et al. 2015), and there may  
392 be some sensitivity of the results presented here to these parameterizations. Further investigation  
393 into the factors influencing the simulation of SO variability is an important direction for future  
394 research.

395 *Acknowledgments.* This work was funded by a Frontiers of Earth System Dynamics grant from  
396 the US National Science Foundation (FESD-1338814). We thank Doug Kinnison for providing

397 the WACCM-SD ozone data. We made use of the Iris Python package (Met Office 2010 - 2016)  
398 for data analysis and visualization. We are also grateful for the feedback of Yavor Kostov and two  
399 anonymous reviewers. Data from the simulations analyzed here is available from the authors upon  
400 request.

## 401 **References**

402 Bitz, C. M., and L. M. Polvani, 2012: Antarctic climate response to stratospheric ozone de-  
403 pletion in a fine resolution ocean climate model. *Geophys. Res. Lett.*, **39**, L20705, doi:  
404 10.1029/2012GL053393.

405 Ciasto, L. M., and D. W. J. Thompson, 2008: Observations of large-scale ocean-atmosphere inter-  
406 action in the Southern Hemisphere. *J. Clim.*, **21**, 1244–1259, doi:10.1175/2007JCLI1809.1.

407 Cionni, I., and Coauthors, 2011: Ozone database in support of CMIP5 simulations: results  
408 and corresponding radiative forcing. *Atmos. Chem. Phys.*, **11**, 11267–11292, doi:10.5194/  
409 acp-11-11267-2011.

410 Comiso, J. C., and F. Nishio, 2008: Trends in the sea ice cover using enhanced and compat-  
411 ible AMSR-E, SSM/I, and SMMR data. *J. Geophys. Res. Ocean.*, **113**, 1–22, doi:10.1029/  
412 2007JC004257.

413 de Lavergne, C., J. B. Palter, E. D. Galbraith, R. Bernardello, and I. Marinov, 2014: Cessation of  
414 deep convection in the open Southern Ocean under anthropogenic climate change. *Nat. Clim.*  
415 *Chang.*, **4**, 278–282, doi:10.1038/nclimate2132.

416 Dunne, J. P., and Coauthors, 2012: GFDL’s ESM2 Global Coupled Climate-Carbon Earth System  
417 Models. Part I: Physical Formulation and Baseline Simulation Characteristics. *J. Clim.*, **25**,  
418 6646–6665, doi:10.1175/JCLI-D-11-00560.1.

419 Ferreira, D., J. Marshall, C. M. Bitz, S. Solomon, and A. Plumb, 2015: Antarctic Ocean and  
420 Sea Ice Response to Ozone Depletion: A Two-Time-Scale Problem. *J. Clim.*, **28**, 1206–1226,  
421 doi:10.1175/JCLI-D-14-00313.1.

422 Fox-Kemper, B., R. Ferrari, and R. Hallberg, 2008: Parameterization of Mixed Layer Eddies. Part  
423 I: Theory and Diagnosis. *J. Phys. Oceanogr.*, **38**, 1145–1165, doi:10.1175/2007JPO3788.1.

424 Galbraith, E. D., and Coauthors, 2011: Climate Variability and Radiocarbon in the CM2Mc Earth  
425 System Model. *J. Clim.*, **24**, 4230–4254, doi:10.1175/2011JCLI3919.1.

426 Gent, P. R., 2016: Effects of Southern Hemisphere Wind Changes on the Meridional  
427 Overturning Circulation in Ocean Models. *Ann. Rev. Mar. Sci.*, 79–94, doi:10.1146/  
428 annurev-marine-122414-033929.

429 Gent, P. R., and J. C. McWilliams, 1990: Isopycnal Mixing in Ocean Circulation Models. *J. Phys.*  
430 *Oceanogr.*, **20**, 150–155.

431 Gerber, E. P., and S.-W. Son, 2014: Quantifying the Summertime Response of the Austral Jet  
432 Stream and Hadley Cell to Stratospheric Ozone and Greenhouse Gases. *J. Clim.*, **27**, 5538–  
433 5559, doi:10.1175/JCLI-D-13-00539.1.

434 Gnanadesikan, A., M.-A. Pradal, and R. Abernathy, 2015: Isopycnal mixing by mesoscale eddies  
435 significantly impacts oceanic anthropogenic carbon uptake. *Geophys. Res. Lett.*, **42**, 4249–4255,  
436 doi:10.1002/2015GL064100.

437 Goosse, H., W. Lefebvre, A. de Montety, E. Cressin, and A. H. Orsi, 2009: Consistent past half-  
438 century trends in the atmosphere, the sea ice and the ocean at high southern latitudes. *Clim.*  
439 *Dyn.*, **33**, 999–1016, doi:10.1007/s00382-008-0500-9.

- 440 Grise, K. M., L. M. Polvani, G. Tselioudis, Y. Wu, and M. D. Zelinka, 2013: The ozone hole  
441 indirect effect: Cloud-radiative anomalies accompanying the poleward shift of the eddy-driven  
442 jet in the Southern Hemisphere. *Geophys. Res. Lett.*, **40**, 3688–3692, doi:10.1002/grl.50675.
- 443 Hall, A., and M. Visbeck, 2002: Synchronous Variability in the Southern Hemisphere Atmosphere  
444 , Sea Ice , and Ocean Resulting from the Annular Mode. *J. Clim.*, **15**, 3043–3057.
- 445 Hande, L. B., S. T. Siems, and M. J. Manton, 2012: Observed Trends in Wind Speed over the  
446 Southern Ocean. *Geophys. Res. Lett.*, **39**, L11 802, doi:10.1029/2012GL051734.
- 447 Heuzé, C., J. K. Ridley, D. Calvert, D. P. Stevens, and K. J. Heywood, 2015: Increasing vertical  
448 mixing to reduce Southern Ocean deep convection in NEMO3.4. *Geosci. Model Dev.*, **8**, 3119–  
449 3130, doi:10.5194/gmd-8-3119-2015.
- 450 Kjellsson, J., and Coauthors, 2015: Model sensitivity of the Weddell and Ross seas, Antarctica,  
451 to vertical mixing and freshwater forcing. *Ocean Model.*, **94**, 141–152, doi:10.1016/j.ocemod.  
452 2015.08.003.
- 453 Kostov, Y., J. Marshall, U. Hausmann, K. C. Armour, D. Ferreira, and M. M. Holland, 2016: Fast  
454 and slow responses of southern ocean sea surface temperature to sam in coupled climate models.  
455 *Climate Dynamics*, 1–15, doi:10.1007/s00382-016-3162-z.
- 456 Large, W. G., J. C. McWilliams, and S. C. Doney, 1994: Oceanic Vertical Mixing - a Review  
457 and a Model with a Nonlocal Boundary-Layer Parameterization. *Rev. Geophys.*, **32**, 363–403,  
458 doi:10.1029/94rg01872.
- 459 Large, W. G., and S. G. Yeager, 2009: The global climatology of an interannually varying air–sea  
460 flux data set. *Clim. Dyn.*, **33**, 341–364, doi:10.1007/s00382-008-0441-3.

461 Lefebvre, W., and H. Goosse, 2008: An analysis of the atmospheric processes driving the large-  
462 scale winter sea ice variability in the Southern Ocean. *J. Geophys. Res.*, **113**, C02 004, doi:  
463 10.1029/2006JC004032.

464 Lefebvre, W., H. Goosse, R. Timmermann, and T. Fichefet, 2004: Influence of the Southern  
465 Annular Mode on the sea ice–ocean system. *J. Geophys. Res.*, **109**, C09 005, doi:10.1029/  
466 2004JC002403.

467 Marshall, J., K. C. Armour, J. R. Scott, Y. Kostov, U. Hausmann, D. Ferreira, T. G. Shepherd, and  
468 C. M. Bitz, 2014: The ocean’s role in polar climate change: asymmetric Arctic and Antarctic  
469 responses to greenhouse gas and ozone forcing. *Philos. Trans. R. Soc. A*, **372**, 20130 040, doi:  
470 10.1098/rsta.2013.0040.

471 Martin, T., W. Park, and M. Latif, 2013: Multi-centennial variability controlled by South-  
472 ern Ocean convection in the Kiel Climate Model. *Clim. Dyn.*, **40**, 2005–2022, doi:10.1007/  
473 s00382-012-1586-7.

474 Meijers, A. J. S., E. Shuckburgh, N. Bruneau, J. B. Sallee, T. J. Bracegirdle, and Z. Wang, 2012:  
475 Representation of the Antarctic Circumpolar Current in the CMIP5 climate models and future  
476 changes under warming scenarios. *J. Geophys. Res.*, **117**, C12 008, doi:10.1029/2012JC008412.

477 Met Office, 2010 - 2016: *Iris: A Python library for analysing and visualising meteorological and*  
478 *oceanographic data sets*. Exeter, Devon, v1.9 ed., URL <http://scitools.org.uk/>.

479 Neely, R. R., D. R. Marsh, K. L. Smith, S. M. Davis, and L. M. Polvani, 2014: Biases in southern  
480 hemisphere climate trends induced by coarsely specifying the temporal resolution of strato-  
481 spheric ozone. *Geophys. Res. Lett.*, **41**, doi:10.1002/2014GL061627.

482 Parkinson, C. L., and D. J. Cavalieri, 2012: Antarctic sea ice variability and trends, 1979-2010.  
483 *Cryosph.*, **6**, 871–880, doi:10.5194/tc-6-871-2012.

484 Polvani, L. M., D. W. Waugh, G. J. P. Correa, and S.-W. Son, 2011: Stratospheric Ozone Deple-  
485 tion: The Main Driver of Twentieth-Century Atmospheric Circulation Changes in the Southern  
486 Hemisphere. *J. Clim.*, **24**, 795–812, doi:10.1175/2010JCLI3772.1.

487 Pradal, M.-A., and A. Gnanadesikan, 2014: How does the Redi parameter formsoscalemixing  
488 impact global climate in an Earth System Model? *J. Adv. Model. Earth Syst.*, **6**, 586–601, doi:  
489 10.1002/2013MS000273.

490 Previdi, M., L. M. Polvani, and M. Previdi, 2014: Climate system response to stratospheric ozone  
491 depletion and recovery. *Q. J. R. Meteorol. Soc. Q. J. R. Meteorol. Soc.*, **140**, 2401–2419, doi:  
492 10.1002/qj.2330.

493 Purich, A., W. Cai, M. H. England, and T. Cowan, 2016: Evidence for link between modelled  
494 trends in Antarctic sea ice and underestimated westerly wind changes. *Nat. Commun.*, **7**, 10 409,  
495 doi:10.1038/ncomms10409.

496 Redi, M., 1982: Oceanic isopycnal mixing by coordinate rotation. *J. Phys. Oceanogr.*, **12**, 1154–  
497 1158, doi:10.1175/1520-0485(1983)013<1318:OIMBCR>2.0.CO;2.

498 Sen Gupta, A., and M. H. England, 2006: Coupled ocean-atmosphere-ice response to variations  
499 in the southern annular mode. *J. Clim.*, **19**, 4457–4486, doi:10.1175/JCLI3843.1.

500 Sigmund, M., and J. C. Fyfe, 2010: Has the ozone hole contributed to increased Antarctic sea ice  
501 extent? *Geophys. Res. Lett.*, **37**, L18 502, doi:10.1029/2010GL044301.

502 Sigmund, M., and J. C. Fyfe, 2014: The Antarctic Sea Ice Response to the Ozone Hole in Climate  
503 Models. *J. Clim.*, **27**, 1336–1342, doi:10.1175/JCLI-D-13-00590.1.

504 Smith, K. L., L. M. Polvani, and D. R. Marsh, 2012: Mitigation of 21st century Antarctic  
505 sea ice loss by stratospheric ozone recovery. *Geophys. Res. Lett.*, **39**, L20701, doi:10.1029/  
506 2012GL053325.

507 Solomon, A., L. M. Polvani, K. L. Smith, and R. P. Abernathy, 2015a: The impact of ozone  
508 depleting substances on the circulation, temperature, and salinity of the Southern Ocean: An  
509 attribution study with CESM1(WACCM). *Geophys. Res. Lett.*, **42** (13), 5547–5555, doi:10.  
510 1002/2015GL064744.

511 Solomon, S., D. Kinnison, J. Bandoro, and R. Garcia, 2015b: Simulation of polar ozone depletion:  
512 An update. *J. Geophys. Res.*, **120**, 7958–7974, doi:10.1002/2015JD023365.

513 Swart, N. C., and J. C. Fyfe, 2012: Observed and simulated changes in the Southern Hemisphere  
514 surface westerly wind-stress. *Geophys. Res. Lett.*, **39**, 6–11, doi:10.1029/2012GL052810.

515 Thomas, J. L., D. Waugh, and A. Gnanadesikan, 2015: Decadal variability in the Southern Hemi-  
516 sphere extratropical circulation: Recent trends and natural variability. *Geophys. Res. Lett.*, **42**,  
517 5508–5515, doi:10.1002/2015GL064521.

518 Thompson, D. W. J., and S. Solomon, 2002: Interpretation of recent Southern Hemisphere climate  
519 change. *Science*, **296**, 895–899, doi:10.1126/science.1069270.

520 Thompson, D. W. J., S. Solomon, P. J. Kushner, M. H. England, K. M. Grise, and D. J. Karoly,  
521 2011: Signatures of the Antarctic ozone hole in Southern Hemisphere surface climate change.  
522 *Nat. Geosci.*, **4**, 741–749, doi:10.1038/ngeo1296.

523 Turner, J., T. J. Bracegirdle, T. Phillips, G. J. Marshall, and J. Scott Hosking, 2013: An initial  
524 assessment of antarctic sea ice extent in the CMIP5 models. *J. Clim.*, **26**, 1473–1484, doi:  
525 10.1175/JCLI-D-12-00068.1.

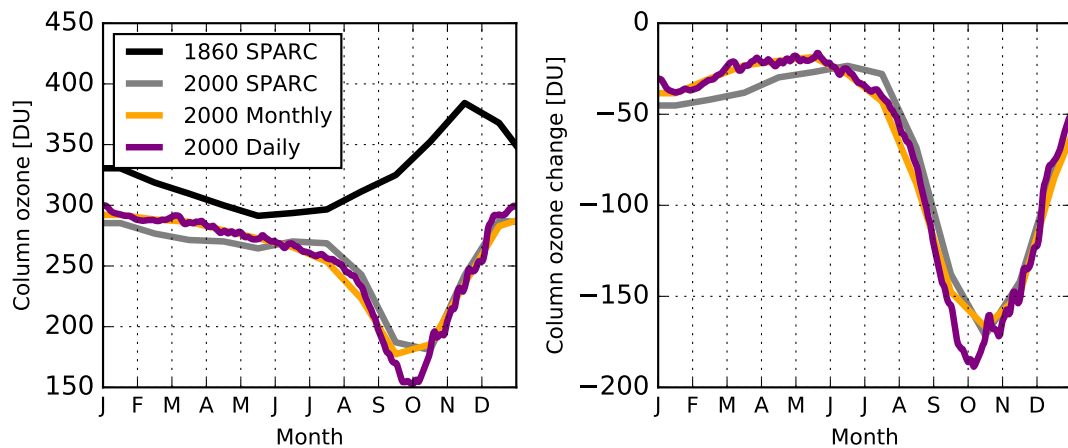
- 526 Watterson, I. G., 2000: Southern midlatitude zonal wind vacillation and its interaction with the  
527 ocean in GCM simulations. *J. Clim.*, **13**, 562–578.
- 528 Zhang, S., M. J. Harrison, A. Rosati, and A. Wittenberg, 2007: System Design and Evaluation of  
529 Coupled Ensemble Data Assimilation for Global Oceanic Climate Studies. *Mon. Weather Rev.*,  
530 **135**, 3541–3564, doi:10.1175/MWR3466.1.

531  
532  
533  
534  
535  
536  
  
537  
538  
539  
540  
541  
  
542  
543  
544  
545  
546  
547  
548  
  
549  
550  
  
551  
552  
553  
  
554  
555  
556  
557  
558  
559  
  
560  
561  
562  
563  
564  
  
565  
566  
567  
  
568  
569  
570  
571  
572  
573

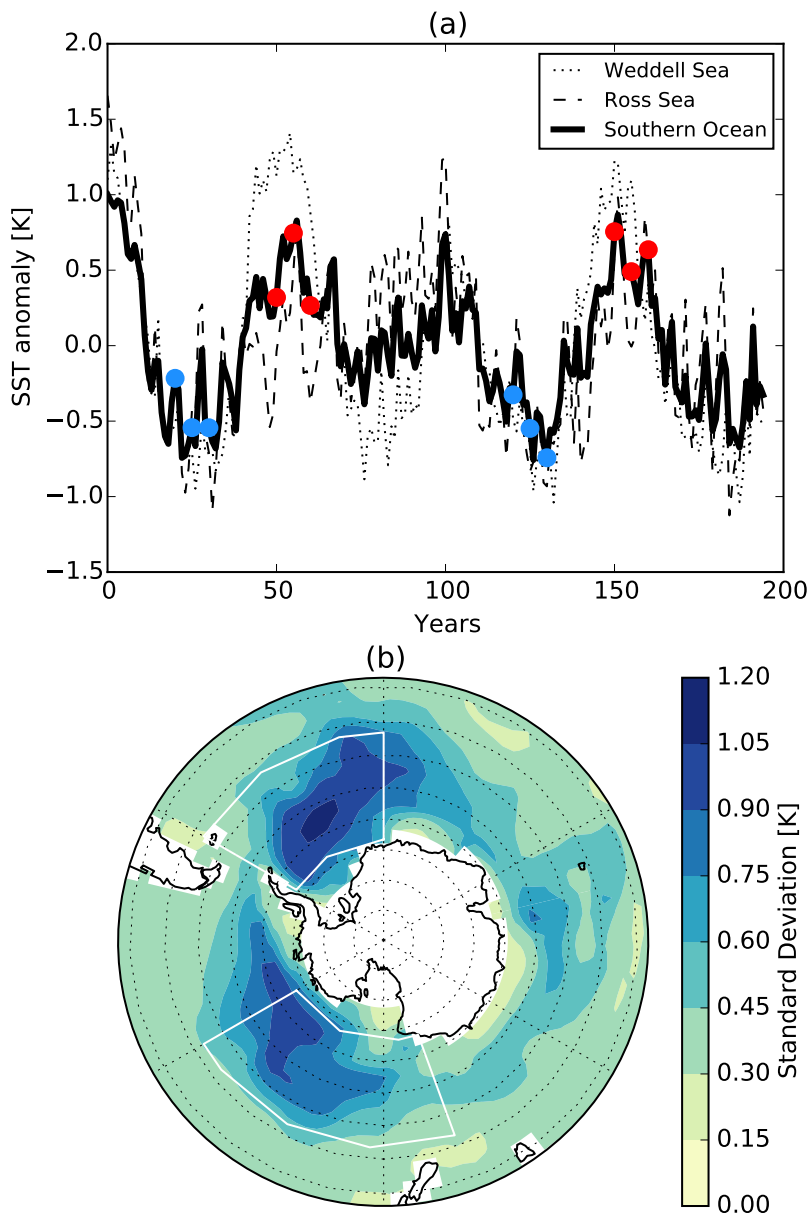
## LIST OF FIGURES

<b>Fig. 1.</b>	(left) Seasonal cycle of polar cap (70-90°S) averaged column ozone in the control simulation (1860 SPARC) and the perturbation simulations with year 2000 ozone prescribed with monthly- and daily-mean values from WACCM-SD. (right) Difference of 2000 ozone and 1860 ozone simulations. Also shown for comparison is 2000 column ozone from the SPARC dataset, and the difference between 2000 and 1860 SPARC values (gray line, right).	27
<b>Fig. 2.</b>	(a) Annual-mean Southern Ocean (50-70°S), Ross Sea (50-75°S, 160°E-120°W), and Weddell Sea (50-75°S, 60-0°W) averaged SST from the preindustrial control simulation. Red dots show the initialization dates for the ‘warm start’ ozone depletion simulations and blue dots show the ‘cold start’ initialization dates. (b) Interannual standard deviation of SST from the same simulation. White boxes show the Ross Sea and Weddell Sea regions.	28
<b>Fig. 3.</b>	(a) Annual average zonal-mean zonal wind stress anomalies, averaged over the 48 years of the ozone perturbation simulations, for the ensemble mean, cold and warm start ensembles, and daily and monthly mean ozone ensembles. Vertical dashed line shows the location of maximum wind stress in the control simulation. (b) Variation of zonal-mean zonal wind-stress with time for the ensemble mean. (c) Zonal wind stress anomalies (colors) and climatology from the control simulation (black contours). The contour interval is 50 mPa, and anomalies are calculated relative to the control simulation.	29
<b>Fig. 4.</b>	Ensemble mean zonal mean SST response. Anomalies are calculated relative to the control simulation.	30
<b>Fig. 5.</b>	Potential temperature anomaly for the ensemble mean averaged over the Southern Ocean (50°-70°S). The solid and dashed black lines show the mixed-layer depth, averaged over December-February and June-August respectively.	31
<b>Fig. 6.</b>	(a) Ensemble average, annual-mean Eulerian MOC streamfunction response, $\Psi'_{\text{Eul}}$ (Sv, black), and potential temperature, $\Theta$ (K, color). The contour interval is 2 K for temperature, and 0.25 Sv for the streamfunction. Solid lines denote a clockwise circulation, dashed counterclockwise. (b) Annual-mean response of the Eulerian ( $\Psi'_{\text{Eul}}$ , solid) and residual mean ( $\Psi'_{\text{Res}}$ , dashed) MOC at 200 m, showing the ensemble average as well as daily and monthly ozone ensembles.	32
<b>Fig. 7.</b>	Annual mean temperature anomaly at 62°S, 200 m for the daily- and monthly-mean ozone simulations as well as the ensemble average. Anomalies are calculated relative to the climatology of the control simulation. The dashed line shows the linear best fit to the ensemble average, and the horizontal line represents the value of the ensemble mean SST anomaly (multiplied by $-1$ ) between 50-70°S over the first 20 years.	33
<b>Fig. 8.</b>	Southern Ocean (50-70S) SST anomaly relative to the climatology of the pre-ozone depletion control simulation, split into daily- and monthly-mean ozone and warm and cold start ensembles. SST evolution is dominated by the initial state.	34
<b>Fig. 9.</b>	Southern Ocean (50-70S) average SST following 10 warm (red) and 11 cold (blue) years sampled from a 500-year control simulation. Shaded regions represent the 95% confidence interval on the expected response calculated from the autocorrelation function. Years are selected from the control simulation which are at least one standard deviation from the mean and spaced at least 5 years apart, in order to mirror the selection of start dates for the ozone response simulations.	35

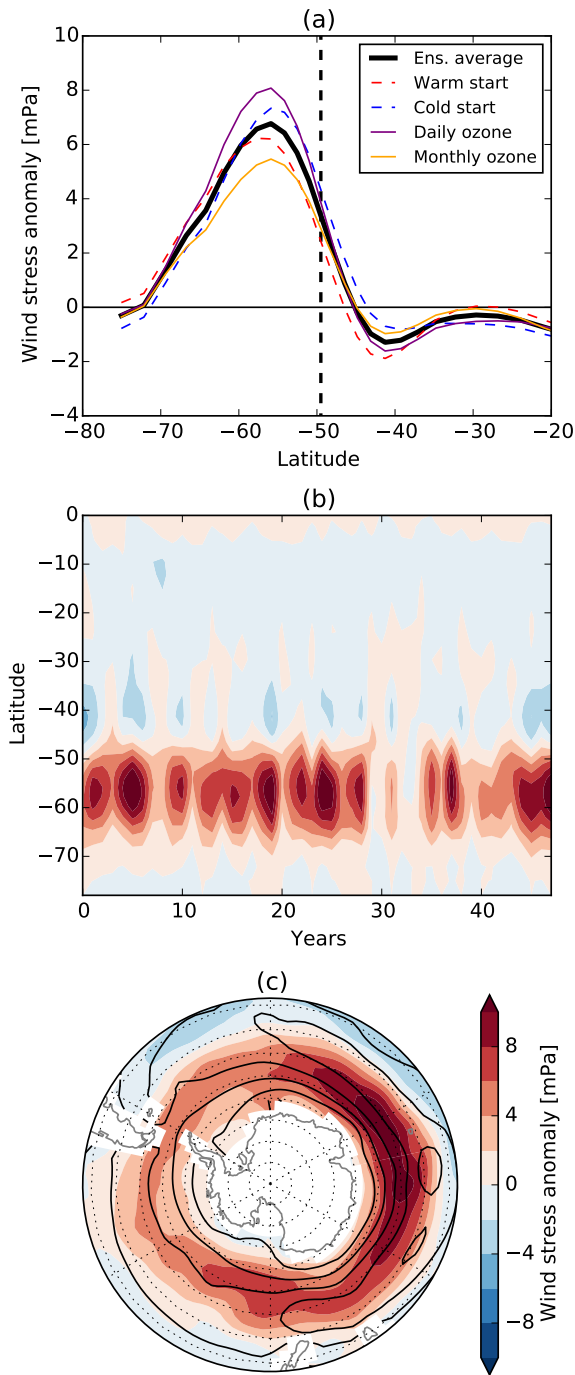
574	<b>Fig. 10.</b>	(a,c,e) Response of Southern Ocean, Ross Sea, and Weddell Sea SST to the ozone perturbation. Year zero represents the initial conditions, and year one is the first year after the perturbation is applied. The shaded region represents the 95% confidence interval on the expected response in the absence of a perturbation, calculated from the autocorrelation of a 500-year control simulation. (b,d,f) Differences of the simulated response from this expected natural variability, bold lines show where this difference lies outside the interval of natural variability. . . . .	36
575			
576			
577			
578			
579			
580			
581	<b>Fig. 11.</b>	SST anomaly of the ensemble mean perturbation simulations relative to the climatology of the pre-ozone depletion control simulation, for 0-15, 15-30, and 30-45 years following ozone depletion. Gray boxes show the Ross and Weddell Sea regions. . . . .	37
582			
583			
584	<b>Fig. 12.</b>	Winter (July-August) sea ice anomaly of the ensemble mean perturbation simulations relative to the climatology of the pre-ozone depletion control simulation, for 0-15, 15-30, and 30-45 years following ozone depletion. . . . .	38
585			
586			
587	<b>Fig. 13.</b>	Sea ice anomaly of the ensemble mean perturbation simulations relative to the pre-ozone depletion control simulation. Sea ice area is calculated by summing the fraction of sea ice in each grid cell multiplied by the area of that grid cell. . . . .	39
588			
589			



590 FIG. 1. (left) Seasonal cycle of polar cap (70-90°S) averaged column ozone in the control simulation (1860  
 591 SPARC) and the perturbation simulations with year 2000 ozone prescribed with monthly- and daily-mean values  
 592 from WACCM-SD. (right) Difference of 2000 ozone and 1860 ozone simulations. Also shown for comparison  
 593 is 2000 column ozone from the SPARC dataset, and the difference between 2000 and 1860 SPARC values (gray  
 594 line, right).



595 FIG. 2. (a) Annual-mean Southern Ocean (50-70°S), Ross Sea (50-75°S, 160°E-120°W), and Weddell Sea  
 596 (50-75°S, 60-0°W) averaged SST from the preindustrial control simulation. Red dots show the initialization  
 597 dates for the ‘warm start’ ozone depletion simulations and blue dots show the ‘cold start’ initialization dates. (b)  
 598 Interannual standard deviation of SST from the same simulation. White boxes show the Ross Sea and Weddell  
 599 Sea regions.



600 FIG. 3. (a) Annual average zonal-mean zonal wind stress anomalies, averaged over the 48 years of the ozone  
 601 perturbation simulations, for the ensemble mean, cold and warm start ensembles, and daily and monthly mean  
 602 ozone ensembles. Vertical dashed line shows the location of maximum wind stress in the control simulation.  
 603 (b) Variation of zonal-mean zonal windstress with time for the ensemble mean. (c) Zonal wind stress anomalies  
 604 (colors) and climatology from the control simulation (black contours). The contour interval is 50 mPa, and  
 605 anomalies are calculated relative to the control simulation.

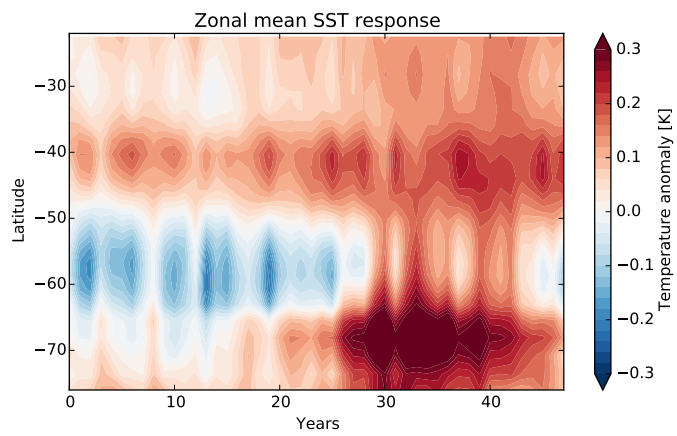
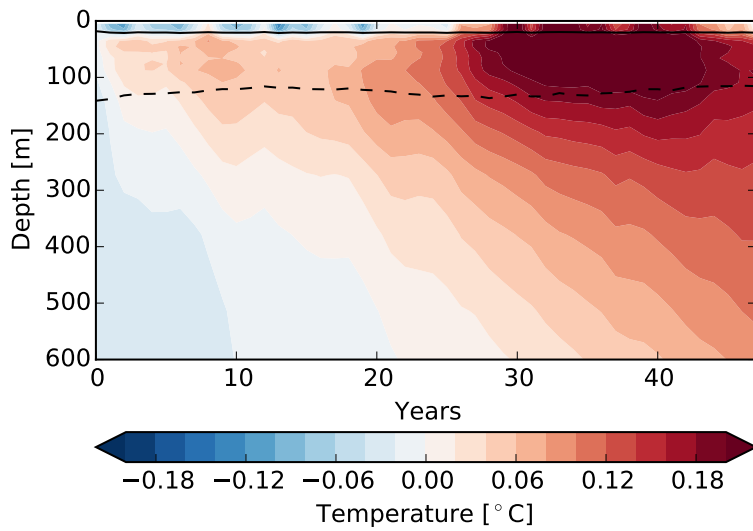
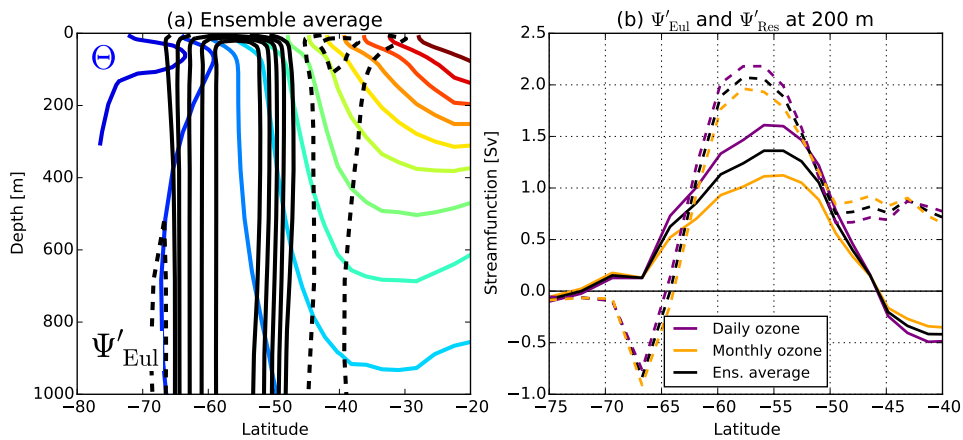


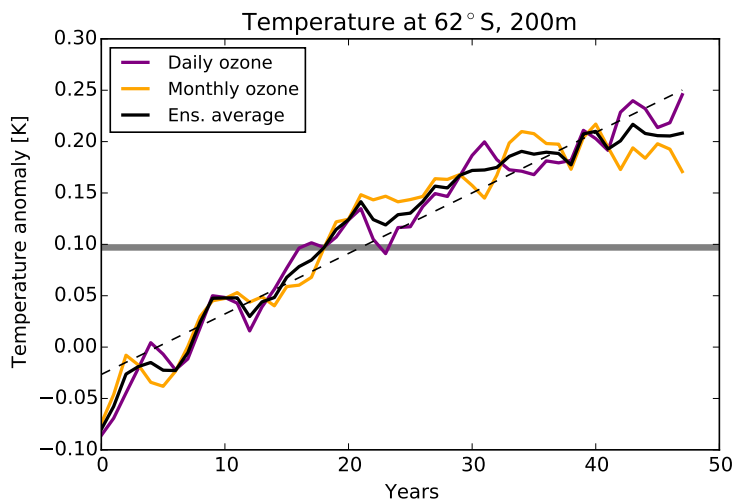
FIG. 4. Ensemble mean zonal mean SST response. Anomalies are calculated relative to the control simulation.



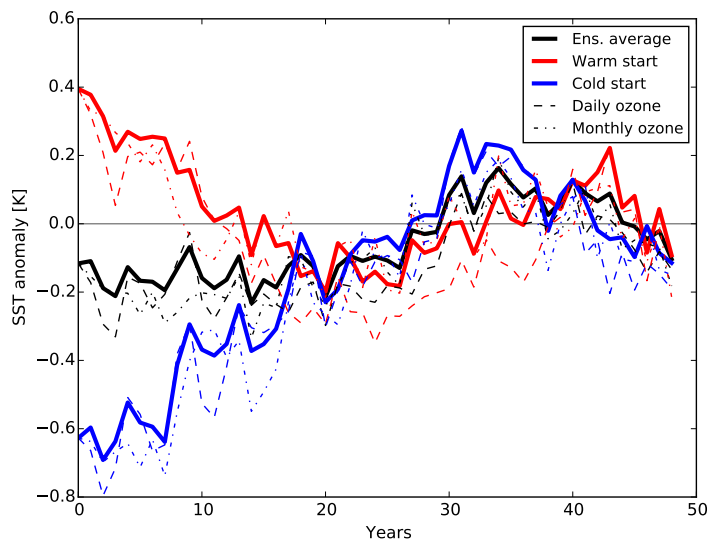
606 FIG. 5. Potential temperature anomaly for the ensemble mean averaged over the Southern Ocean (50°-70°S).  
 607 The solid and dashed black lines show the mixed-layer depth, averaged over December-February and June-  
 608 August respectively.



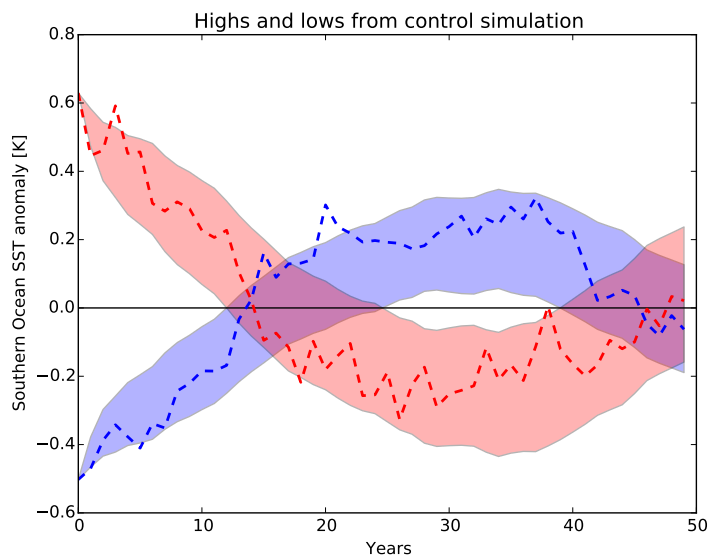
609 FIG. 6. (a) Ensemble average, annual-mean Eulerian MOC streamfunction response,  $\Psi'_{Eul}$  (Sv, black), and  
 610 potential temperature,  $\Theta$  (K, color). The contour interval is 2 K for temperature, and 0.25 Sv for the stream-  
 611 function. Solid lines denote a clockwise circulation, dashed counterclockwise. (b) Annual-mean response of the  
 612 Eulerian ( $\Psi'_{Eul}$ , solid) and residual mean ( $\Psi'_{Res}$ , dashed) MOC at 200 m, showing the ensemble average as well as  
 613 daily and monthly ozone ensembles.



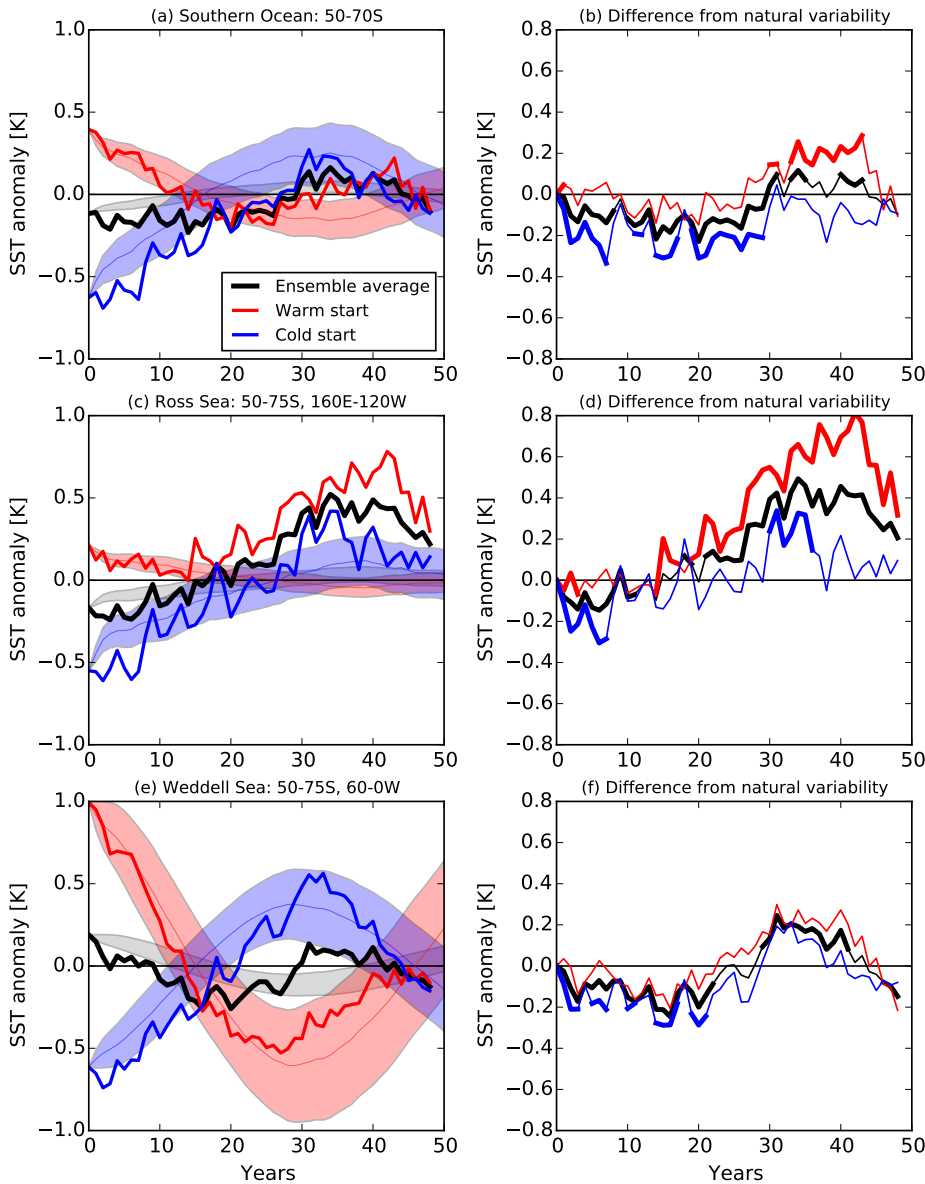
614 FIG. 7. Annual mean temperature anomaly at 62°S, 200 m for the daily- and monthly-mean ozone simulations  
 615 as well as the ensemble average. Anomalies are calculated relative to the climatology of the control simulation.  
 616 The dashed line shows the linear best fit to the ensemble average, and the horizontal line represents the value of  
 617 the ensemble mean SST anomaly (multiplied by  $-1$ ) between 50-70°S over the first 20 years.



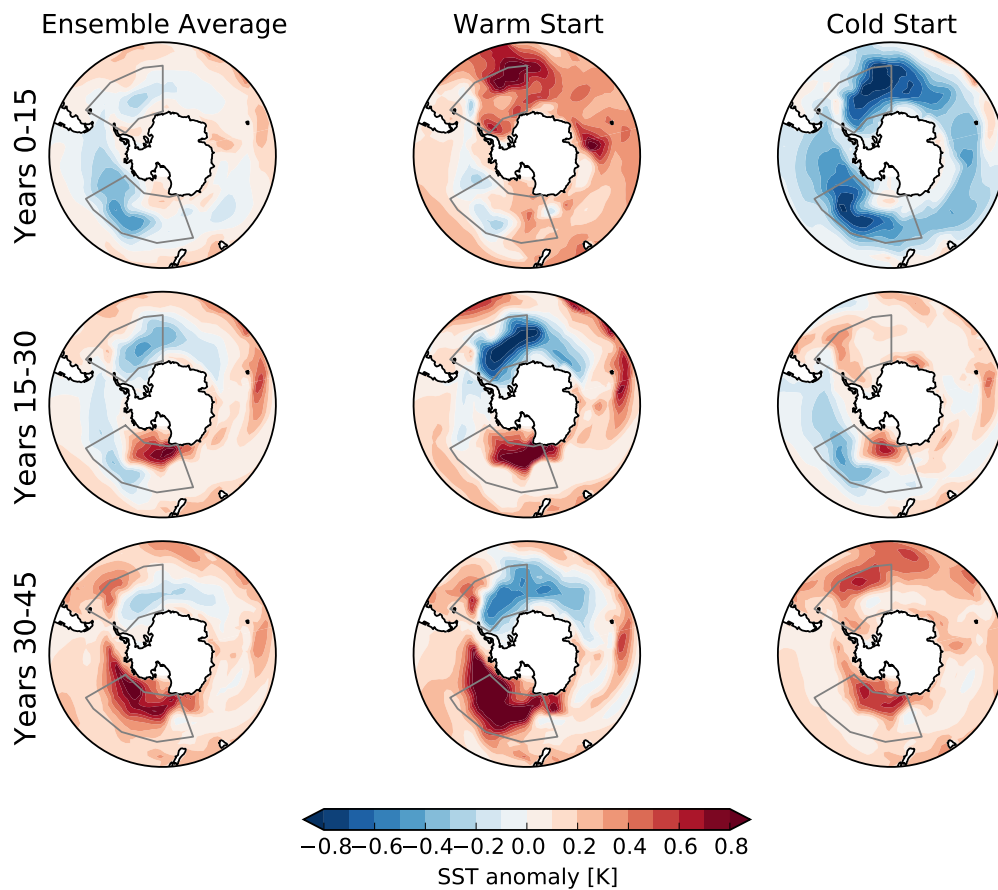
618 FIG. 8. Southern Ocean (50-70S) SST anomaly relative to the climatology of the pre-ozone depletion control  
 619 simulation, split into daily- and monthly-mean ozone and warm and cold start ensembles. SST evolution is  
 620 dominated by the initial state.



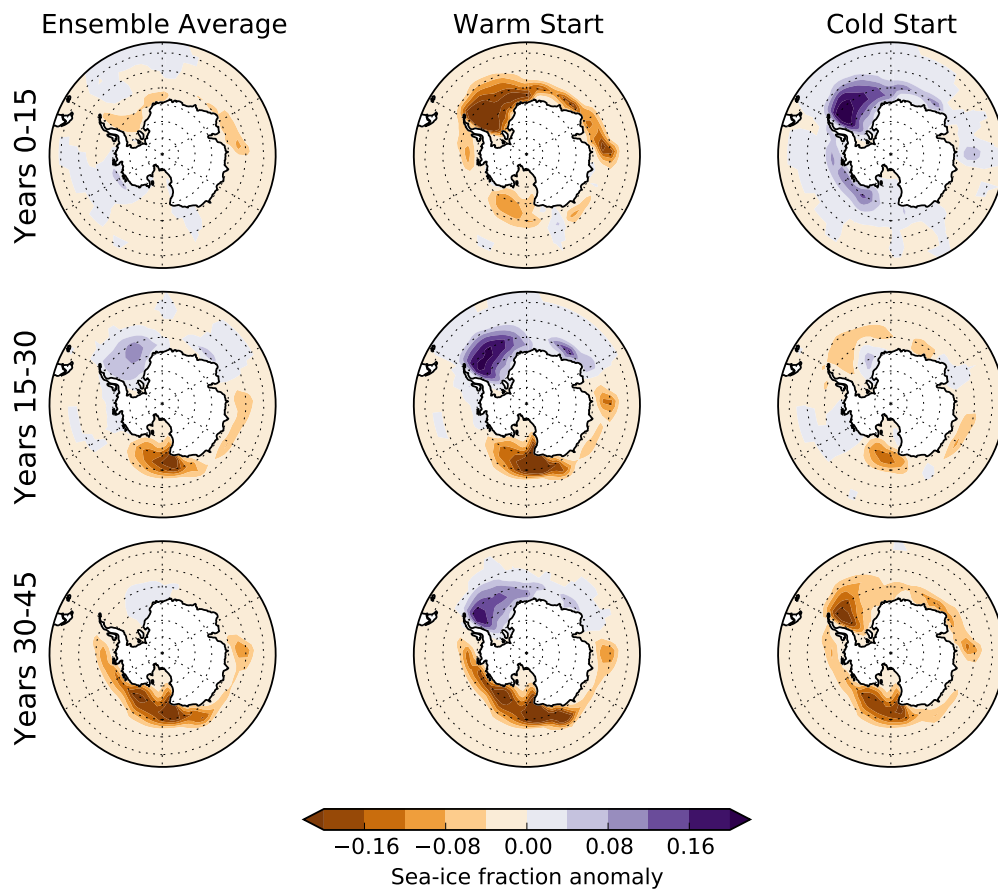
621 FIG. 9. Southern Ocean (50-70S) average SST following 10 warm (red) and 11 cold (blue) years sampled from  
 622 a 500-year control simulation. Shaded regions represent the 95% confidence interval on the expected response  
 623 calculated from the autocorrelation function. Years are selected from the control simulation which are at least  
 624 one standard deviation from the mean and spaced at least 5 years apart, in order to mirror the selection of start  
 625 dates for the ozone response simulations.



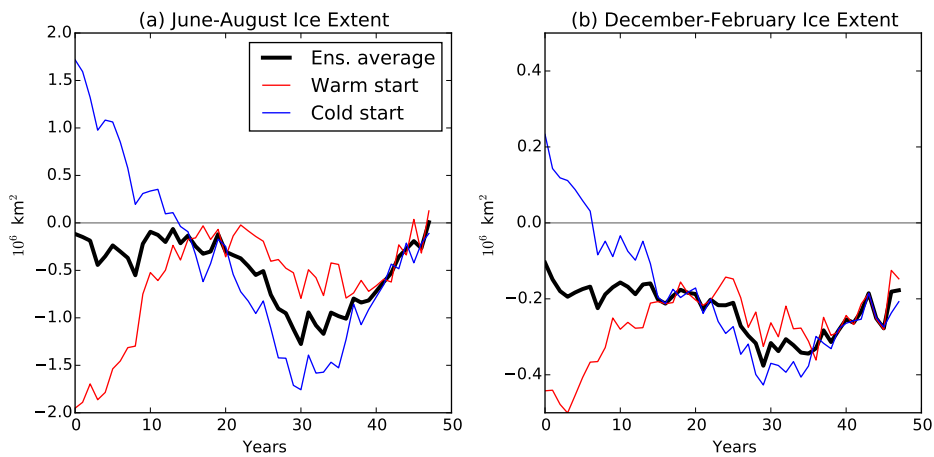
626 FIG. 10. (a,c,e) Response of Southern Ocean, Ross Sea, and Weddell Sea SST to the ozone perturbation. Year  
 627 zero represents the initial conditions, and year one is the first year after the perturbation is applied. The shaded  
 628 region represents the 95% confidence interval on the expected response in the absence of a perturbation, calcu-  
 629 lated from the autocorrelation of a 500-year control simulation. (b,d,f) Differences of the simulated response  
 630 from this expected natural variability, bold lines show where this difference lies outside the interval of natural  
 631 variability.



632 FIG. 11. SST anomaly of the ensemble mean perturbation simulations relative to the climatology of the pre-  
 633 ozone depletion control simulation, for 0-15, 15-30, and 30-45 years following ozone depletion. Gray boxes  
 634 show the Ross and Weddell Sea regions.



635 FIG. 12. Winter (July-August) sea ice anomaly of the ensemble mean perturbation simulations relative to the  
 636 climatology of the pre-ozone depletion control simulation, for 0-15, 15-30, and 30-45 years following ozone  
 637 depletion.



638 FIG. 13. Sea ice anomaly of the ensemble mean perturbation simulations relative to the pre-ozone depletion  
 639 control simulation. Sea ice area is calculated by summing the fraction of sea ice in each grid cell multiplied by  
 640 the area of that grid cell.